

## WAVELENGTH ACCURACY OF THE KECK HIRES SPECTROGRAPH AND MEASURING CHANGES IN THE FINE STRUCTURE CONSTANT

KIM GRIEST<sup>1</sup>, JONATHAN B. WHITMORE<sup>1</sup>, ARTHUR M. WOLFE<sup>1,6</sup>, J. XAVIER PROCHASKA<sup>2,3,6</sup>, J. CHRISTOPHER HOWK<sup>4,6</sup>,  
AND GEOFFREY W. MARCY<sup>5</sup>

<sup>1</sup> Department of Physics, University of California, San Diego, CA 92093, USA; kgriest@ucsd.edu, jonathan.b.whitmore@gmail.com

<sup>2</sup> University of California Observatories - Lick Observatory, University of California, Santa Cruz, CA 95064, USA

<sup>3</sup> Department of Astronomy and Astrophysics, University of California, Santa Cruz, Santa Cruz, CA 95064, USA

<sup>4</sup> Department of Physics, University of Notre Dame, Notre Dame, IN 46616, USA

<sup>5</sup> Department of Astronomy, University of California, Mail Code 3411, Berkeley, CA 94720, USA

Received 2009 April 29; accepted 2009 November 3; published 2009 December 9

### ABSTRACT

We report on an attempt to accurately wavelength calibrate four nights of data taken with the Keck HIRES spectrograph on QSO PHL957, for the purpose of determining whether the fine structure constant was different in the past. Using new software and techniques, we measured the redshifts of various Ni II, Fe II, Si II, etc. lines in a damped Ly $\alpha$  system at  $z = 2.309$ . Roughly half the data were taken through the Keck iodine cell which contains thousands of well calibrated iodine lines. Using these iodine exposures to calibrate the normal Th–Ar Keck data pipeline output, we found absolute wavelength offsets of  $500 \text{ m s}^{-1}$  to  $1000 \text{ m s}^{-1}$  with drifts of more than  $500 \text{ m s}^{-1}$  over a single night, and drifts of nearly  $2000 \text{ m s}^{-1}$  over several nights. These offsets correspond to an absolute redshift of uncertainty of about  $\Delta z \approx 10^{-5}$  ( $\Delta\lambda \approx 0.02 \text{ \AA}$ ), with daily drifts of around  $\Delta z \approx 5 \times 10^{-6}$  ( $\Delta\lambda \approx 0.01 \text{ \AA}$ ), and multiday drifts of nearly  $\Delta z \approx 2 \times 10^{-5}$  ( $\approx 0.04 \text{ \AA}$ ). The causes of the wavelength offsets are not known, but since claimed shifts in the fine structure constant would result in velocity shifts of less than  $100 \text{ m s}^{-1}$ , this level of systematic uncertainty may make it difficult to use Keck HIRES data to constrain the change in the fine structure constant. Using our calibrated data, we applied both our own fitting software and standard fitting software to measure  $\frac{\Delta\alpha}{\alpha}$ , but discovered that we could obtain results ranging from significant detection of either sign, to strong null limits, depending upon which sets of lines and which fitting method were used. We thus speculate that the discrepant results on  $\frac{\Delta\alpha}{\alpha}$  reported in the literature may be due to random fluctuations coming from underestimated systematic errors in wavelength calibration and fitting procedure.

*Key words:* atomic data – cosmological parameters – instrumentation: spectrographs – quasars: absorption lines – techniques: spectroscopic

*Online-only material:* color figures

### 1. INTRODUCTION: VARYING FINE STRUCTURE CONSTANT

The fine structure constant today,  $\alpha_0 = 1/137.03599911$ , is usually thought of as a fundamental, unchanging, constant of nature, but recently both experimental and theoretical papers have challenged this assumption, (e.g., see the review by Garcia-Berro et al. 2007). Motivated especially by the possible experimental detection (see below) of a change in  $\alpha$ , we applied for and took four nights of Keck data, half of it through the Keck iodine cell, on quasi-stellar object (QSO) PHL957. Our goal was to get an extremely well-calibrated, high signal/noise (S/N) absorption spectrum on a distant damped Ly $\alpha$  (DLA) system ( $z = 2.309$ ) in order to measure the value of the fine structure constant more than 10 billion years ago and compare it to the value today.

The basic method to determine  $\frac{\Delta\alpha}{\alpha} = (\alpha_z - \alpha_0)/\alpha_0$  is to measure differences in redshifts between different atomic transitions of elements in the same physical system, and use the fact that for small changes in  $\alpha$  the energy level of a given atomic transition can be approximated as

$$\omega_\alpha = \omega_0 + 2q \frac{\Delta\alpha}{\alpha}, \quad (1)$$

where  $\omega_0 = 1/\lambda_0$  is the frequency of the transition on Earth,  $\omega_\alpha$  is the frequency in the high redshift cloud, and the  $q$ -values measure the dependence of  $\omega_\alpha$  on  $\alpha$  and have been calculated for many common transitions. (see, for example, Murphy et al. 2001a; Dzuba et al. 2002, and Porsev et al. 2007 for more detailed discussion and Table 2 for the values of  $q$  for various transitions.) The values of  $q$  depend upon the electron orbital configurations of the initial and final quantum states, and therefore different transitions have different values of  $q$ . If all transitions had the same  $q$ , then all wavelength shifts would be the same, and one could absorb any change in  $\alpha$  into the determination of the redshift of the physical system. However, since different transitions have different values of  $q$ , the relative transition wavelengths will differ from what they are in the lab if  $\frac{\Delta\alpha}{\alpha} \neq 0$ .

For example, Murphy et al. (2001a, 2001b, 2003, 2004) used a many-multiplet method on Keck HIRES data of 143 absorption systems in the redshift range  $0.2 < z < 3.7$  to find a significant reduction of  $\alpha$  in the past,  $\frac{\Delta\alpha}{\alpha} = (-5.43 \pm 1.16) \times 10^{-6}$ , while Chand et al. (2004) and Srianand et al. (2004) used the same method for a subset of transitions on VLT/UVES data on 23 absorbers to find  $\frac{\Delta\alpha}{\alpha} = (-0.6 \pm 0.6) \times 10^{-6}$ . This latter analysis was criticized by Murphy et al. (2008b) who reanalyzed the Chand et al. data to get  $\frac{\Delta\alpha}{\alpha} = (-4.4 \pm 3.6) \times 10^{-6}$ , consistent with their previous result. In the meantime other groups returned results, for example, Levshakov et al. (2006) used the

<sup>6</sup> Visiting Astronomer, W. M. Keck Telescope. The Keck Observatory is a joint facility of the University of California and the California Institute of Technology.

VLT/UVES spectrograph to study Fe II lines in one system at  $z = 1.15$  and found a null result,  $\frac{\Delta\alpha}{\alpha} = (-.07 \pm 0.84) \times 10^{-6}$ , and in another system at  $z = 1.8$  to find  $\frac{\Delta\alpha}{\alpha} = (5.4 \pm 2.5) \times 10^{-6}$  (Levshakov et al. 2007). Murphy et al. (2008a) have also criticized these results, claiming that the data do not allow limits as strong as those reported. Subsequently, the Levshakov et al. (2006) results were weakened to  $\frac{\Delta\alpha}{\alpha} = (-0.12 \pm 1.8) \times 10^{-6}$  for the  $z = 1.15$  system and  $\frac{\Delta\alpha}{\alpha} = (5.7 \pm 2.7) \times 10^{-6}$  for the  $z = 1.8$  system (Molaro et al. 2008), still a null result inconsistent with the detections.

Given the above inconsistent results, we were particularly interested in the Fe II  $\lambda 1608$  and Fe II  $\lambda 1611$  transitions since these have  $q$  values that are both large and more importantly of opposite sign. Thus, if  $\alpha$  was different in the past, the relative positions of these two lines should be significantly shifted from their laboratory values. For our DLA at  $z = 2.309$ , a relative shift between Fe II  $\lambda 1608$  and Fe II  $\lambda 1611$  of about  $-136 \pm 21 \text{ m s}^{-1}$  is expected if the Murphy et al. value  $\frac{\Delta\alpha}{\alpha} = (-5.43 \pm 0.116) \times 10^{-6}$  is correct. (Fe II  $\lambda 1608$  shifts by  $-54 \pm 12 \text{ m s}^{-1}$ , while Fe II  $\lambda 1611$  shifts by  $82 \pm 18 \text{ m s}^{-1}$  in the rest frame.) Thus, our goal was to centroid these lines to better than  $50 \text{ m s}^{-1}$ , so as to determine  $\frac{\Delta\alpha}{\alpha}$  in a single ion in a single absorption system.

Our method, which is close to that used by Levshakov et al. 2006, contrasts with that of Murphy et al. (2001a, 2001b, 2003, 2004) and Chand et al. (2004) where the S/N was not high enough to detect the  $\frac{\Delta\alpha}{\alpha}$  signal in any single pair of lines; they did a statistical averaging over many transitions in many absorption systems, and thus might be subject to systematic errors in selection, calibration, or averaging procedures. Since we expected to have superbly well-calibrated spectra, and these two Fe II lines appear in the same echelle order, we hoped that we could give convincing evidence for or against a change in the fine structure constant.

For our work, in addition to the Fe II lines, there are also several Ni II, Si II, Al II, and Al III lines that fall in the wavelength range covered by the iodine cell and that we can use. In what follows, besides the Fe II  $\lambda 1608/\lambda 1611$  pair, various other sets of lines are used. Potentially, we could fit all 16 lines that have calculated  $q$  values and that appear in our spectra: Fe II  $\lambda 1608/\lambda 1611/\lambda 2344$ , Ni II  $\lambda 1709/\lambda 1741/\lambda 1751$ , Si II  $\lambda 1526/\lambda 1808$ , Al III  $\lambda 1854/\lambda 1862$ , Al II  $\lambda 1670$ , Cr II  $\lambda 2062/\lambda 2056/\lambda 2066$ , and Zn II  $\lambda 2026/\lambda 2062$ . If we restrict ourselves to lines that occur at wavelengths for which we have iodine spectra, we would use only the nine lines: Fe II  $\lambda 1608/\lambda 1611$ , Ni II  $\lambda 1709/\lambda 1741/\lambda 1751$ , Si II  $\lambda 1808$ , Al III  $\lambda 1854/\lambda 1862$ , and Al II  $\lambda 1670$ . If we worry that saturated lines (those with minimum flux less than 10%) may not be accurately fit, we can restrict ourselves to the seven lines that meet the above criteria and are unsaturated: Fe II  $\lambda 1611$ , Ni II  $\lambda 1709/\lambda 1741/\lambda 1751$ , Si II  $\lambda 1808$ , and Al III  $\lambda 1854/\lambda 1862$ . Finally, we note that Al III has a systematically higher ionization potential than the other ions and is a sub-dominant ionization state of Al. It thus could exist in a physically different location. Thus, we most reliably consider the five calibratable, unsaturated, singly ionized transitions: Fe II  $\lambda 1611$ , Ni II  $\lambda 1709/\lambda 1741/\lambda 1751$ , and Si II  $\lambda 1808$ .

## 2. DATA AND EXTRACTION

PHL957 is a bright ( $B = 16.6$ ) quasi-stellar object (QSO) at  $z = 2.7$ , with a damped Ly $\alpha$  system at  $z = 2.309$  (Beaver et al. 1972). We obtained 5.5 hr of data on 2002 November 1, 4 hr on 2004 October 3, 4 hr on 2004 October 4, and 5 hr on

2004 October 5. Five of the 11 exposures taken in 2002 had the iodine cell in place, while six of the 13 exposures taken in 2004 were taken through the iodine cell. Table 1 shows how the iodine cell exposures were interspersed with the non-iodine cell exposures. Table 1 also shows the times that the relevant Th/Ar calibration arcs were taken, as well the temperatures inside the HIRES enclosure, and whether or not the echelle gratings were moved between the QSO exposures and the relevant Th/Ar exposures. The data from 2002 were acquired through the C1 decker (FWHM  $\approx 6 \text{ km s}^{-1}$ ), with the kv380 blocking filter in place. The data from 2004 were also observed through the C1 decker but with the kv418 blocking filter, and the CCD mosaic was binned by two in the spatial dimension.

The 2002 spectra were extracted and combined using MAKEE (Barlow 2002). The 2004 spectra were extracted and combined using the XIDL<sup>7</sup> package HIRedux<sup>8</sup> (Bernstein et al., in preparation). The 2002 and 2004 data cannot be easily combined since a new mosaic of CCD's was installed in the spectrograph in between these runs. We note that the 2002 data have a substantially worse S/N pixel<sup>-1</sup> (42 for the non-iodine cell exposures) compared to the combined 2004 non-iodine cell data which have a S/N of about 70 pixel<sup>-1</sup>.

### 2.1. Iodine Cell

The Keck iodine cell has been used extensively in searches for extra solar planets using the Doppler technique (Butler et al. 1996). The cell is placed in the beam and superposes several narrow absorption lines per Angstrom on the QSO spectrum between 4950 Å and 5900 Å. As pointed out by Murphy et al. (2001b), the different optical paths of the Th–Ar lamp and the QSO spectrum are a possible source of the systematic error in the wavelength calibration. Using the iodine cell, wavelength calibration errors can be dramatically reduced since issues such as atmospheric dispersion, guiding errors at the slit, and all changes to the optics of the spectrograph are shared by both the iodine lines and the QSO spectra. In addition, the Th–Ar lamp spectra are done at different times than the QSO spectra.

Figure 1 shows a sample of the iodine cell spectra taken with the Fourier transform spectrometer (FTS) at Kitt Peak National Observatory (KPNO) with a resolution of around 170,000 and a S/N of 700 pixel<sup>-1</sup> (Butler et al. 1996; G. W. Marcy 2008, unpublished). This high resolution and S/N means that we do not expect the iodine spectrum to be a significant source of wavelength calibration error. Figure 2 shows a portion of echelle order 67 taken both with and without the iodine cell. In the bottom panel of Figure 2, one can see the iodine lines as well as the Fe II  $\lambda 1608$  and Fe II  $\lambda 1611$  lines of the DLA towards PHL957. The top panel of Figure 2 does not contain the iodine lines.

### 2.2. Wavelength Calibration

In order to do the wavelength calibration, we started from the XIDL Th–Ar calibration.<sup>9</sup> XIDL takes Th–Ar wavelengths that have been transformed from vacuum values to air values so that lines can be identified. Using these identified lines, a polynomial is fit over the full two-dimensional spectrum. The wavelength scale found is then transformed back to vacuum values using the inverse Edlen formula.

<sup>7</sup> <http://www.ucolick.org/~xavier/IDL>

<sup>8</sup> [http://www.ucolick.org/~xavier/HIRedux/HIRES\\_doc.html](http://www.ucolick.org/~xavier/HIRedux/HIRES_doc.html)

<sup>9</sup> As a check, we also extracted spectra using MAKEE, both with and without the sky line wavelength calibration option. In both the cases, iodine re-calibration of about the same magnitude as with XIDL was needed.

**Table 1**  
Journal of PHL957 Observations

| Date       | ID       | Iodine Cell? | Time (UT) | Exposure (s) | Tempin <sup>a</sup> (°C) | Arc ID            | Arc Time (UT) | Moved? <sup>b</sup> | $\Delta$ Tempin (°C) |
|------------|----------|--------------|-----------|--------------|--------------------------|-------------------|---------------|---------------------|----------------------|
| 2002 Nov 1 | 33       | Out          | 5:26      | 1800         | 3.75                     |                   |               |                     |                      |
| 2002 Nov 1 | 34       | Out          | 5:58      | 1800         | 3.76                     |                   |               |                     |                      |
| 2002 Nov 1 | 35       | In           | 6:30      | 1800         | 3.79                     |                   |               |                     |                      |
| 2002 Nov 1 | 36       | In           | 7:01      | 1800         | 3.76                     |                   |               |                     |                      |
| 2002 Nov 1 | 47       | Out          | 7:58      | 1800         | 3.61                     |                   |               |                     |                      |
| 2002 Nov 1 | 48       | Out          | 8:30      | 1800         | 3.68                     |                   |               |                     |                      |
| 2002 Nov 1 | 49       | In           | 9:03      | 1800         | 3.68                     |                   |               |                     |                      |
| 2002 Nov 1 | 50       | In           | 9:34      | 1800         | 3.78                     |                   |               |                     |                      |
| 2002 Nov 1 | 60       | Out          | 10:34     | 1800         | 3.71                     |                   |               |                     |                      |
| 2002 Nov 1 | 61       | Out          | 11:06     | 1800         | 3.75                     |                   |               |                     |                      |
| 2002 Nov 1 | 62       | In           | 11:39     | 1800         | 3.71                     |                   |               |                     |                      |
| 2004 Oct 3 | 67/3-0   | Out          | 9:18      | 3600         | 4.26                     | 66                | 09:15         | no                  | 0.042                |
| 2004 Oct 3 | 68/3-1   | In           | 10:31     | 3600         | 4.21                     | 66                | 09:15         | no                  | 0.097                |
| 2004 Oct 3 | 69/3-2   | In           | 11:33     | 3600         | 4.07                     | 66                | 09:15         | no                  | 0.236                |
| 2004 Oct 3 | 70/3-3   | Out          | 12:35     | 3600         | 4.00                     | 66                | 09:15         | no                  | .0306                |
| 2004 Oct 4 | 1096/4-0 | Out          | 9:25      | 3600         | 3.00                     | 1144              | 15:35         | yes                 | -0.153               |
| 2004 Oct 4 | 1098/4-1 | In           | 10:56     | 3600         | 2.97                     | 1144              | 16:35         | yes                 | -0.125               |
| 2004 Oct 4 | 1099/4-2 | In           | 11:57     | 3600         | 3.01                     | 1144              | 16:35         | yes                 | -0.167               |
| 2004 Oct 4 | 1100/4-3 | Out          | 12:58     | 3600         | 2.93                     | 1144              | 16:35         | yes                 | -0.083               |
| 2004 Oct 5 | 2094/5-0 | In           | 8:25      | 3600         | 2.87                     | 2026              | 3:01          | yes                 | 0.125                |
| 2004 Oct 5 | 2095/5-1 | Out          | 9:27      | 3600         | 2.86                     | 2107              | 15:46         | yes                 | 0.430                |
| 2004 Oct 5 | 2096/5-2 | Out          | 10:29     | 3600         | 2.91                     | 2107              | 15:46         | yes                 | 0.375                |
| 2004 Oct 5 | 2097/5-3 | In           | 11:30     | 3600         | 3.62                     | 2107 <sup>c</sup> | 15:46         | yes                 | -0.333               |
| 2004 Oct 5 | 2098/5-4 | Out          | 12:32     | 2700         | 3.55                     | 2107              | 15:46         | yes                 | -0.264               |

**Notes.**

<sup>a</sup> Temperature inside the the HIRES enclosure.

<sup>b</sup> Whether or not the grating was moved between Th/Ar arc and data exposures.

<sup>c</sup> This exposure was also calibrated with Th Ar arc 2026; see the text.

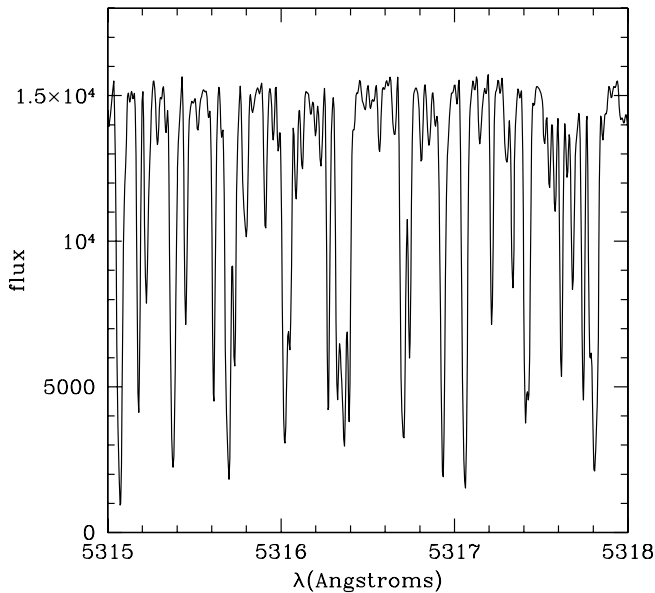


**Figure 1.** 3 Å of the KPNO FTS spectrometer iodine cell spectrum.

After finding the Th–Ar wavelength scale, we use our iodine measurements with two similar but independent methods to recalibrate. In both methods, we convolved the high S/N iodine spectrum measured at KNPO (Butler et al. 1996) with a Gaussian and then minimized the  $\chi^2$  of the difference between this convolved spectrum and the PHL957 spectrum shifted by an amount  $\Delta\lambda_{\text{cal}}$ .

In the first method, a three-parameter fit was performed in each wavelength bin of the PHL957 spectra, with bin sizes from 1 to 10 Å being used. The fit returned the wavelength

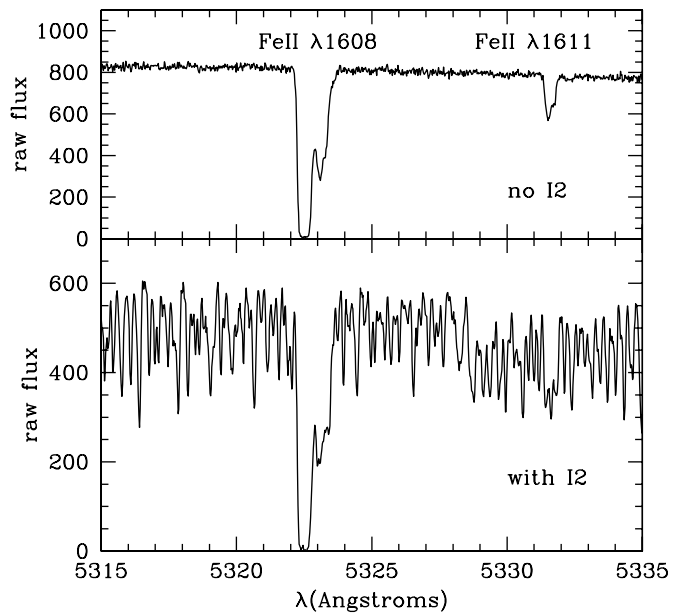


**Figure 2.** Combined 2004 absorption spectra showing a portion of order 67 containing the Fe II  $\lambda$ 1608 and Fe II  $\lambda$ 1611 lines. The top panel shows the spectrum taken without the iodine cell in place, and the bottom panel shows the spectrum taken through the iodine cell.

shift,  $\Delta\lambda_{\text{cal}}$ , the sigma of the convolution Gaussian, as well as a multiplicative continuum offset and the formal errors of these quantities. Using this method, regions of the PHL957 spectra that had strong lines were not included in the fit since these could distort the results; a linear interpolation of bins on either side of the line region was used to find a correction at the line center.

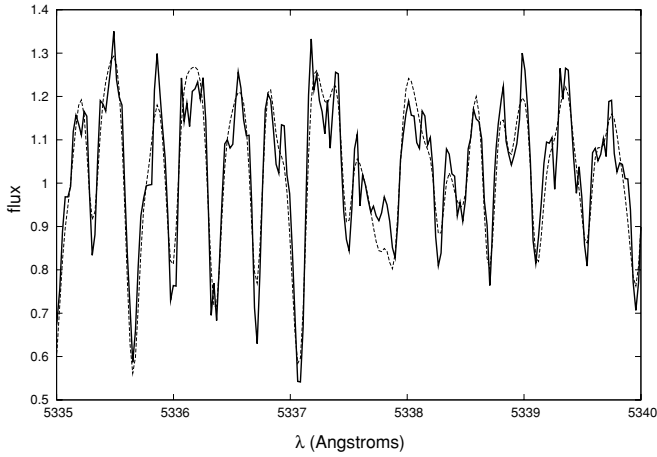


**Figure 3.** Small portion of echelle order 67 of PHL957 (thick line) compared with the convolved and shifted FTS iodine cell spectrum (thin dashed line).

Using the second method, strong lines in the PHL957 spectra were fit and subtracted from the data before differencing with the convolved iodine spectra. This allowed direct determination of a wavelength correction even at line centers (except for saturated regions which are removed as above). Also, in the second method rather than fitting for both  $\Delta\lambda_{\text{cal}}$  and the convolution sigma in each wavelength bin, a rolling 5–10 Å bin iterative method was used that found the wavelength correction for each data point and also the one best convolution sigma for the entire echelle order. We also tried setting the sigma of our Gaussian convolution kernel to the resolution expected from the physical setup of the telescope,  $R = 50,000$ . This sigma was consistent with but slightly smaller than the sigma we found by fitting, but the wavelength offsets found either way agreed to within errors. In this method, the errors in the wavelength calibration were found from the values of  $\Delta\lambda_{\text{cal}}$  that caused the  $\chi^2$  to increase by 1.

The methods of finding the continuum of the FTS iodine spectra were also somewhat different for the two methods. In the first method, we used the highest flux value in a variable size wavelength bin as the continuum value. In the second method, we averaged the three largest flux values (and their corresponding wavelengths) in each 1 Å bin, and then set the continuum by fitting a spline through these averaged points.

Determining the continua of the PHL957 spectra taken with the iodine cell is difficult because of the large number of unresolved overlapping iodine lines. The first method used a fourth-order polynomial fit to the set flux values within  $2\sigma$  of the highest flux found over a certain wavelength range. The second method found the PHL957 continuum using a standard continuum fitting program, thus probably underestimating it. Because of this underestimate, we repeated our analysis using several different possible continua and discovered that our final wavelength calibration results were robust for all plausible PHL957 continua.

A comparison between the results of the two methods showed agreement in  $\Delta\lambda_{\text{cal}}$  within errors and also good agreement in the reported errors on  $\Delta\lambda_{\text{cal}}$ . We also tried a method that used a cross-correlation between the FTS and PHL957 spectra, which also worked, but did not seem as accurate as either of the other two methods.

We will use the results of our second method throughout the rest of the paper. Our final recalibration shift data is smoothed with a 5-Angstrom box filter to reduce fitting noise.

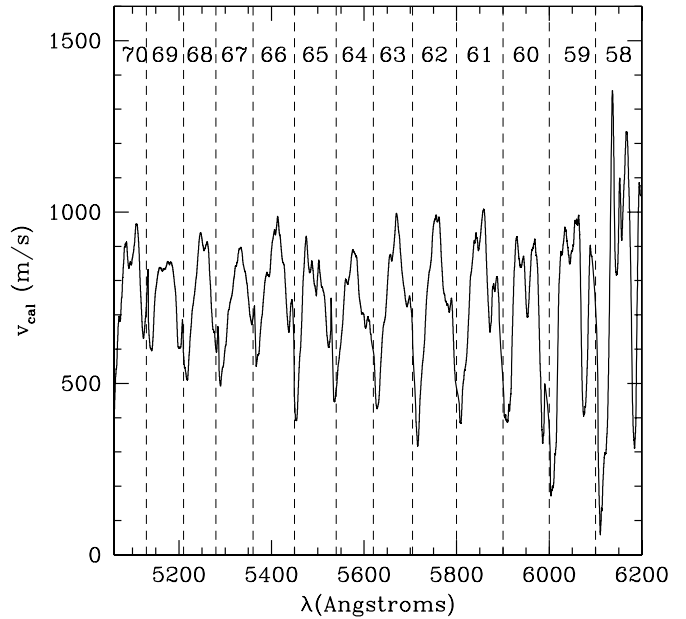


**Figure 4.** Wavelength correction over entire wavelength range for exposure 3-1 of PHL957. The shift is between the standard Th–Ar wavelength calibration and the wavelength scale found by fitting to the FTS iodine spectrum. The echelle order is marked.

Figure 3 compares a small portion of echelle order 67 of PHL957 with the convolved and shifted FTS iodine cell spectrum.

Note that the Th–Ar-calibrated spectra used as input to our recalibration pipeline should not include the standard Keck HIRES heliocentric correction that accounts for the Doppler shift from the changing motion of the Earth around the Sun. We recalibrate in the lab frame, and then make our own, more accurate, solar system barycentric motion correction using the code developed by G. W. Marcy & R. P. Butler (2008, unpublished). This barycentric correction should be good to better than 1 m s<sup>-1</sup>.

We found that the accuracy of the wavelength recalibration as measured by our calculated error depended strongly on the size of the bin used for the convolution. Thus, we report values from a 10 Å bin analysis as a compromise between small uncertainty and constancy of the wavelength calibration over the width of a single bin.

Figure 4 shows an example (exposure 3-1) of the resultant wavelength recalibration shift over the entire wavelength range for which we have both QSO and FTS iodine spectra. This figure is a major result of this work.

We see several interesting effects. First the size of the shift is significant: typically from 500 m s<sup>-1</sup> to 1000 m s<sup>-1</sup> corresponding to a substantial fraction of a CCD pixel (roughly 1300 m s<sup>-1</sup> pixel<sup>-1</sup> or 0.023 Å pixel<sup>-1</sup> at  $\lambda \approx 5300$  Å.) Contrast these systematic velocity errors with an expected shift of 136 m s<sup>-1</sup> (rest frame) between Fe II  $\lambda 1608$  and Fe II  $\lambda 1611$  due to the  $\frac{\Delta\alpha}{\alpha}$  claim described in the introduction. We note previous workers have found similar Keck HIRES shifts of 1000 m s<sup>-1</sup> or larger (e.g., page 734 of the night airglow line paper by Osterbrock et al. 2000), and Figure 4 of Suzuki et al. 2003), but this does not seem to be widely appreciated.

Second, there is a clear pattern seen in each echelle order, with the shift increasing from the edge of each order and reaching a maximum near the middle. For the purpose of measuring  $\frac{\Delta\alpha}{\alpha}$ , it is not the overall shift discussed above that is important,

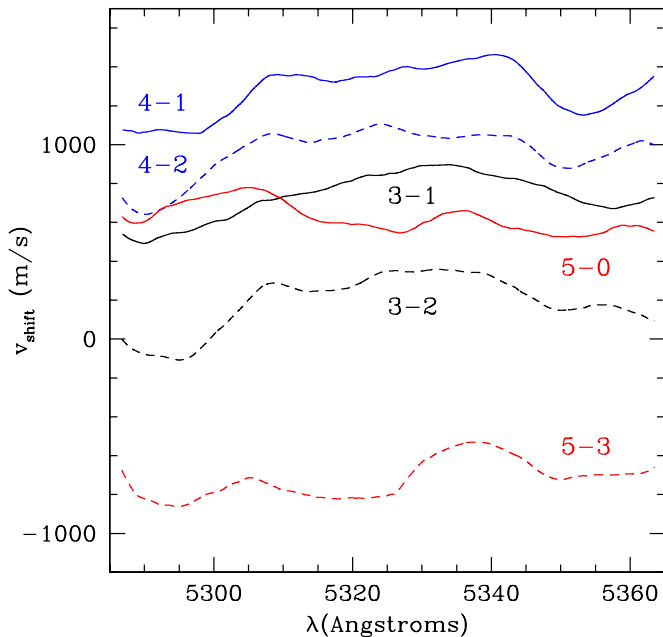


**Figure 5.** Time evolution of iodine cell wavelength recalibration shift for echelle order 67. Each line is labeled by the day-observation number, with the solid line being the exposure taken earlier in the night.

(A color version of this figure is available in the online journal.)

but the relative shift between the transitions being compared. Depending on the echelle order, Figure 4 shows relative shifts of  $300 \text{ m s}^{-1}$  to  $800 \text{ m s}^{-1}$  within the same order. These shifts could be dangerous since, depending upon the lines being compared, they could result in a systematic relative velocity shift between lines, thereby mocking a changing  $\alpha$ .

Next, we are interested in how this wavelength recalibration shift varies with time. Thus, Figure 5 shows a more detailed look at echelle order 67 which contains the Fe II  $\lambda 1608/\lambda 1611$  lines. In the figure, different lines are the recalibration shifts for each of the five exposures that used the iodine cell and are labeled by their ID's, e.g., 3-0 is the first exposure of PHL957 taken on 2004 October 3. See Table 1 for more details.

We note that each exposure has a similar, but not identical shape as a function of wavelength, and that there is a different wavelength offset for each exposure. While the variation over this order for each exposure is typically  $500 \text{ m s}^{-1}$  or less, the shift between different exposures can be as much as  $2000 \text{ m s}^{-1}$ . This means that the Th–Ar wavelength calibration that gives us the wavelength solution as a function of pixel is not stable and drifts with time.

It is of interest to note that recalibration offsets between nights are in general larger than the drifts during each night. One sees that on October 3 and 4, when the iodine cell exposures were taken one after the other, the shift during the night was substantially smaller than the inter-day shifts, while on October 5, when there was 3 hr between iodine cell exposures, there was a larger shift.

Figure 5 is probably more important than the previous figure, since it shows that the Th–Ar calibration is not stable over time. If the wavelength shifts shown in Figure 4 were stable in time, they could be removed and would have little effect on the measurement of  $\frac{\Delta\alpha}{\alpha}$ . But large systematic wavelength shifts during the night mean that measurements at the desired level of precision may be difficult with Th–Ar calibration alone.

It is important to note that even though the calibration errors reported here are much larger than the final velocity

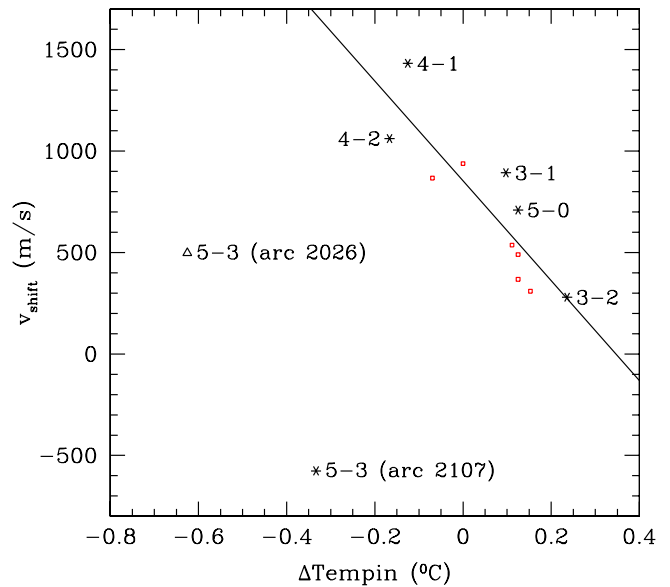


**Figure 6.** Iodine recalibration shift  $v_{\text{shift}}$  vs.  $\Delta\text{Tempin}$  for the PHL957 iodine exposures (labeled asterisks), and a star HD209837 (small squares). The shift is the single best wavelength recalibration shift for echelle order 66 found by our iodine line-fitting program. The quantity  $\Delta\text{Tempin}$  is the temperature inside the HIRES enclosure measured during the Th/Ar arc calibration exposure minus the same temperature measured during the data exposure. The solid trend line,  $v_{\text{shift}} = -2459 \Delta\text{Tempin} + 853$ , is a fit to the points excluding QSO exposure 5-3. Exposure 5-3 appears twice labeled by which Th/Ar calibration arc was used.

(A color version of this figure is available in the online journal.)

precision needed to determine  $\frac{\Delta\alpha}{\alpha}$ , it is possible that these calibration errors average out and do not ruin the final  $\frac{\Delta\alpha}{\alpha}$  determination. In the many multiplet method, many different lines are compared across many different absorbers at many different redshifts. If the signs of the calibration errors are random, the calibration errors may average away. A complete discussion of this possibility is beyond the scope of this work, but will be presented elsewhere.

### 2.3. Understanding the Calibration Shifts

We made some preliminary attempts at understanding the causes of these unexpected wavelength calibration shifts. While complete understanding of the causes and exploration of methods to correct for the shifts are beyond the scope of this paper, we report some ideas and preliminary results here. We hope to use additional data and analysis to find a more complete understanding, which will then be published elsewhere.

First, it is interesting that during all three nights, the shifts became more negative at about  $500 \text{ m s}^{-1}$  per hour. Thus, we plotted the shifts versus time, and also versus the various temperatures, etc. that HIRES reports. With only six iodine exposures, it is difficult to discern a pattern and impossible to prove that a pattern exists, and in fact we did not see any fully convincing trends.

The best partial trend is a decrease in calibration shift with  $\Delta\text{Tempin}$ , where  $\Delta\text{Tempin}$  is the difference in HIRES enclosure temperature between when the Th/Ar calibration exposure was taken and when the QSO exposure was taken. We plot this trend in Figure 6, where the six QSO exposures are shown as asterisks and individually labeled. The data are given in Table 1. We see that the trend is badly broken by the fourth exposure on October 5 (5-3 or ID 2097), which originally led us to discount temperature as the main culprit. However, we have

some exposures of a star (HD209833) taken the same nights through the iodine cell, and we plot the calibration shifts versus  $\Delta\text{Temp}$  for them as small boxes. The complete analysis of these star exposures is beyond the scope of this paper, but we see that they fall on the same trend line, showing that exposure 5-3 seems to be an exception.

Next, we check whether or not the echelle gratings were moved between the time of the Th/Ar arc exposure and the QSO exposure. This is shown in Table 1. We see that only on October 3 (exposures 3-1 and 3-2) the gratings were not moved between Th/Ar calibration and the QSO exposures. In Figure 6, we see that the dispersion of exposures 3-1 and 3-2 from the trend line is smaller than for exposures 4-1 and 4-2. Exposure 5-0 is near the trend line, but of course 5-3 is way off, probably for some other reason. Thus, we see a weak hint that moving the gratings between Th/Ar calibration and science exposure can cause a calibration error.

To understand the problem with exposure 5-3, we note that a different Th/Ar arc was used for 5-3 than for the other iodine exposure (5-0) taken that night. To check whether something went wrong with the arc exposure (ID = 2107) used to calibrate 5-3, we redid the iodine recalibration using arc exposure 2026, taken much earlier that same night. This point is also plotted in Figure 6 as a labeled triangle. The point shifts substantially, but keeps the same (large) distance from the trend line.

Thus, we see that while temperature surely plays an important role and a correction perhaps can be made for this, there are other parameters that seem to be important, not all of which are understood at this point. Moving the gratings between Th/Ar and science exposures may increase the calibration error. In what follows, we will not attempt to use the temperature trend to make any correction, though in future work this might be possible.

We note that other contributions to the calibration shifts are possible. N. Suzuki (2009, private communication) suggested that the cause could be that the HIRES spectrograph is mounted at a small angle with respect to the optical axis, so that the light path rotates as the telescope moves, resulting in variable vignetting in comparison to light from the Th–Ar lamp which is fixed to the spectrograph. More generally, the optical path of the Th/Ar calibration light differs from the optical path of the QSO light resulting in different wavelength to pixel mapping. P. Molaro (2009, private communication) suggested that the cause could be the changing position of the QSO image centroid in the slit. We hope to check this with additional exposures at a future date. M. Murphy (2009, private communication) suggested that the cause could be temperature and pressure differences between the Th/Ar calibration exposures and the data exposures, as well as the resetting of the echelle gratings. The analysis presented above was, in large part, motivated by the comments of M. Murphy.

It would be useful to study and understand these wavelength calibration shifts, perhaps by analyzing other data, since it might then be possible to model and remove them. This will be pursued in more detail elsewhere.

Overall, the wavelength calibration errors reported here may seem to be a remarkable result, but we note that Osterbrock et al., (2000) recalibrated the Keck HIRES Th–Ar tube wavelengths using several night sky airglow lines and found similar ( $\sim 0.05$  Å) calibration errors. In addition, both the magnitude and time variation of these shifts were detected using Ly alpha forest lines by Suzuki et al. (2003).

It is interesting to ask whether sky lines themselves could be used to calibrate the QSO spectra without use of the iodine cell. In fact, the current version of MAKEE data reduction pipeline includes an option to calibrate using sky lines. We used our iodine method to check on the wavelength accuracy of the MAKEE sky line calibration, but still found substantial wavelength shifts both within and across Echelle orders, and as a function of time.

#### 2.4. Use of the Calibration

Our original hope was that if there would be a time-stable wavelength calibration found from the iodine cell exposures then that could be applied to all the exposures. When the iodine cell is in place we get well-calibrated wavelengths, but substantially less S/N. This is because iodine lines cover basically the entire spectrum, decreasing the number of photons, adding spurious components to line-fitting programs, and also making the continuum difficult to determine. So, it is the exposures without the iodine cell that carry the highest S/N and that we wish to use to test for a changing alpha. Since again, as Figure 5 shows, the wavelength calibrations vary substantially over the course of a night, it is not clear how to use the calibration in our fits. We tried several methods before settling on the following: (1) for exposures taken with the iodine cell, we add the wavelength recalibration correction to each wavelength output by the standard HIRES pipeline. (2) For exposures taken without the iodine cell, we interpolate/extrapolate the wavelength correction using the two iodine exposures nearest in time and assuming that the correction changes linearly with time. (3) We then add the barycentric correction to every data point.

At this point, we have wavelength corrected spectra that can be fit. We can either add the spectra for each order together (rebinning since the spectra are no longer on a common wavelength scale) or just combine and sort the data files for each order together with giving more flux measurements to be fit.

We can check the effect of our recalibration by seeing how well sharp features in the spectra line up. For example, Figure 7 shows a close-up of the left edge of the saturated Fe II  $\lambda 1608$  line before and after iodine recalibration. The panel labeled “Th/Ar” (a) shows an overlay of the six iodine exposures calibrated with the standard HIRES pipeline, while the panel labeled “iodine” (a) show the same after our recalibration. The features line up significantly better after recalibration; spreads of more than  $2000 \text{ m s}^{-1}$  become significantly less than  $1000 \text{ m s}^{-1}$ .

The other two panels show overlays of the seven exposures taken without the iodine cell. The panel labeled “Th/Ar” (b) is again the result from the standard HIRES calibration, while the panel labeled ‘Iodine interp’ (b) shows the same seven exposures, but recalibrated using the interpolation scheme described above. For the non-iodine exposures, there is some improvement in alignment of the line edge, but not nearly as much as for the iodine exposures. Here spreads of  $1000 \text{ m s}^{-1}$  or more seem to remain even after recalibration.

Since for S/N and fitting reasons, we must use mainly the non-iodine exposures, it is disappointing that our efforts to recalibrate may not pay off. Our inability to model the calibration shifts between iodine exposures seems to be the main culprit.

### 3. FITTING THE DATA

In what follows, we mostly just combine the recalibrated, continuum-subtracted spectra for all non-iodine exposures into

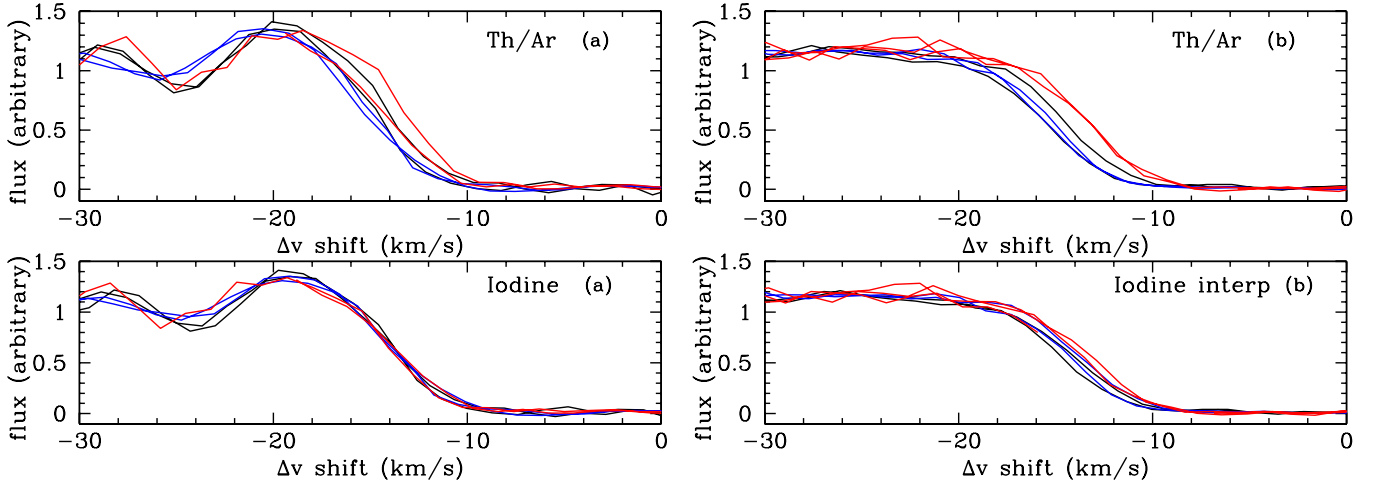


**Figure 7.** Close-ups of the left edge of the Fe II  $\lambda 1608$  line for observations taken on October 3 (black), October 4 (blue), and October 5 (red). The panels labeled “Th/Ar” show results from the standard Th/Ar wavelength calibration, while the panels labeled “Iodine,” or “Iodine interp” show results after recalibration with the iodine cell. The two panels labeled (a) are for the six exposures with the iodine cell in place, while the two panels labeled (b) are for the seven exposures taken without the iodine cell, but recalibrated either using the iodine lines (upper panel) or using interpolation as described in the text (lower panel). The extra bumps in the (a) panels are iodine lines, and the first part of the spectrum in exposure 5-0 is missing due to a cosmic ray. The iodine lines do not line up because of the barycentric correction needed for PHL957.

(A color version of this figure is available in the online journal.)

one large file, and then sort by wavelength and fit. In some cases, we rebin the data combining several data points and adding the errors in quadrature, and in some cases, we just use the co-added spectra from the standard HIRES pipeline. We treat the data from 2002 separately since it was taken on a different CCD chip. We also treat the data with and without the iodine cell separately since the iodine lines add significant effective noise to the PHL957 spectra.

### 3.1. Voigt Profile Fitting

We fit the spectra using a code we developed based upon the CERN library MINUIT minimization program and the humdev Voigt profile calculation routine (Wells 1999). We compared our results with those of VPFIT (Carswell et al. 2008) and DUDE (Kirkman et al. 2003) and found agreement for individual lines. Using our own code allows us easily to do joint fits with the redshifts of transitions varying independently and also allows us to add additional parameters as needed. Figures 8 and 9 show fit results for several transitions for the combined 2004 data. The fit parameters are the redshift, the line width ( $b$ -value), and the column density. We note that several of the lines are saturated, making wavelength centroiding more difficult and less accurate.

### 3.2. Limit on Precision of $\frac{\Delta\alpha}{\alpha}$

The S/N of each 2004 non-iodine spectra is approximately  $25 \text{ pixel}^{-1}$ , giving a total S/N for the seven non-iodine exposures of about  $70 \text{ pixel}^{-1}$ . The individual iodine exposures have a S/N of around  $19 \text{ pixel}^{-1}$ , for a co-added total of about  $47 \text{ pixel}^{-1}$ , though the iodine lines cause the effective S/N to be lower than this. The co-added 2002 data have S/N approximately  $42 \text{ pixel}^{-1}$ . Our total S/N is thus quite high for a high redshift object, and we want to first estimate the minimum possible error on  $\frac{\Delta\alpha}{\alpha}$  that could be obtained with these spectra.

To do this, we use a Fisher matrix-type method suggested by Murphy et al. (2008a), and Bouchy et al. (2001). For continuum-normalized flux spectrum  $F(\lambda_i)$  with  $1\sigma$  error array  $\sigma_F(\lambda_i)$ , the minimum possible uncertainty in velocity contributed by

pixel  $i$  is

$$\frac{\sigma_v(\lambda_i)}{c} = \frac{\sigma_f(\lambda_i)}{\lambda_i(\partial F(\lambda_i)/\partial \lambda_i)}. \quad (2)$$

Thus, more precise velocity measurements come from pixels with large flux gradients and small errors. The minimal possible uncertainty in the velocity of a portion of spectrum is thus

$$\sigma_v = [\sum_i [1/\sigma_v(\lambda_i)]^2]^{-1/2}, \quad (3)$$

where the sum is over pixels. Finally, the minimum uncertainty in  $\frac{\Delta\alpha}{\alpha}$  can be found by performing a least-squares fit to a version of Equation (1)

$$v_j = v_0 + \left(\frac{\Delta\alpha}{\alpha}\right) x_j, \quad x_j = -2cq_j\lambda_{0j}, \quad (4)$$

where  $j$  numbers of the lines that are being compared,  $v_0$  is a constant offset (degenerate with the system redshift), and the minimum error in  $\frac{\Delta\alpha}{\alpha}$  is just the fit uncertainty in the slope of this linear equation.

Murphy et al. (2008a) performed this analysis for their data and for the data of Chand et al. (2004), and Levshakov et al. (2006), finding that while their own errors were (barely) within the allowable minimum, the reported uncertainties of the others were smaller than the minimum possible. The corrected version of the Levshakov results (Molaro et al. 2008) does seem to be in agreement with the minimum error limit.

We would like to perform such an estimate, but first note that previous estimates of minimum errors did not include uncertainties in the  $q$  values. Table 2 shows that these uncertainties can be significant, and inclusion of these uncertainties will increase both the Fisher matrix minimum errors and also the error on  $\frac{\Delta\alpha}{\alpha}$ . One can include these uncertainties,  $\sigma_q(j)$ , in the fit and obtain a more realistic minimum error estimate. In this case, rather than a simple linear least-squares fit one must use a method that allows errors in both the ordinate and the abscissa. Since the uncertainties in  $q$  are theoretical estimates and not statistical errors, this method is not technically completely consistent, but

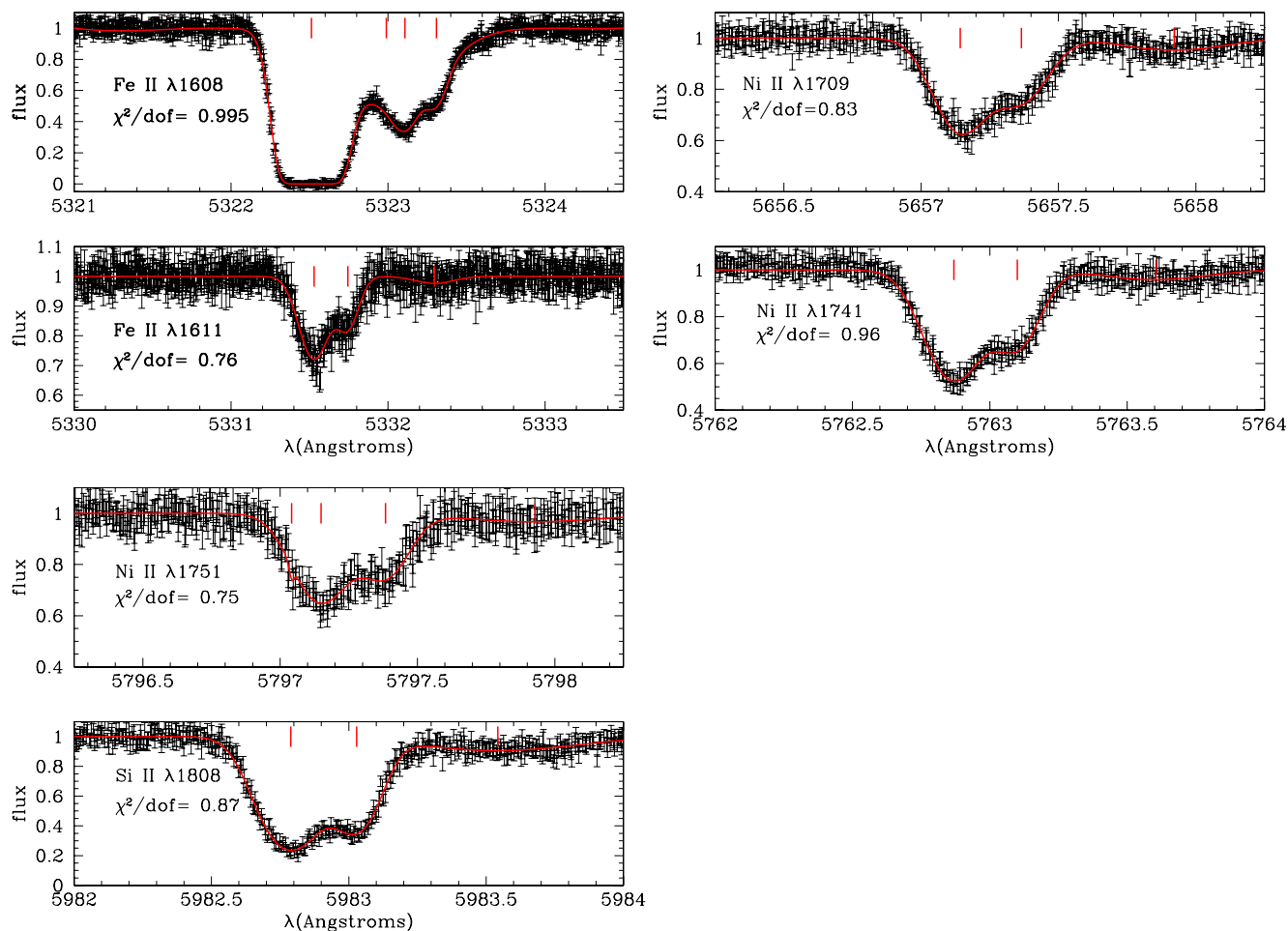


**Figure 8.** Voigt profile fit results for several PHL957 lines using our fitting code. The velocity components are marked. These are unconstrained fits for each line so the velocity components of various transitions are not forced to agree with each other in these plots.

(A color version of this figure is available in the online journal.)

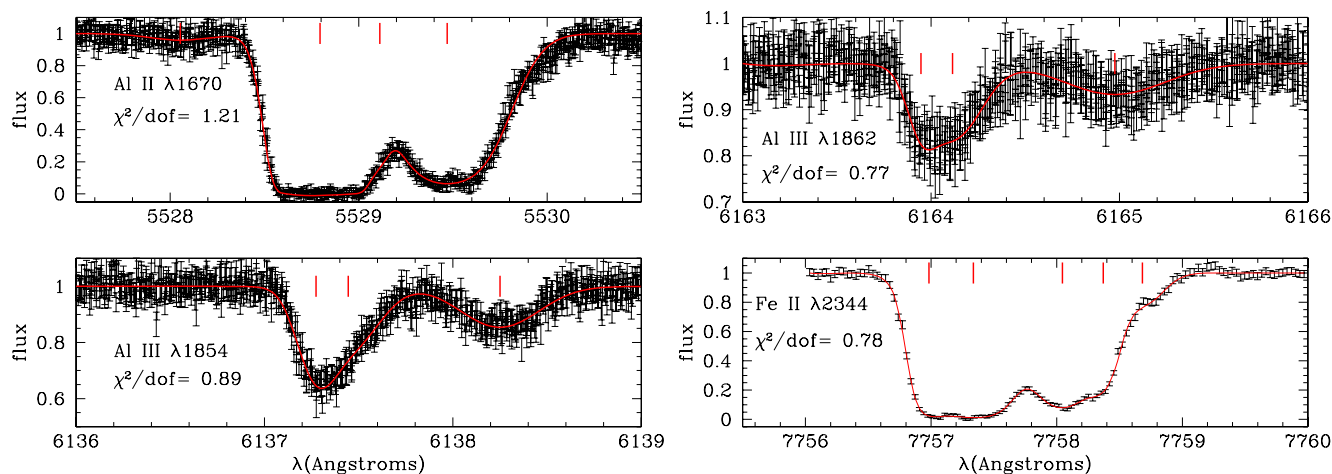


**Figure 9.** Voigt profile fit results for several PHL957 lines using our fitting code. The velocity components are marked.

(A color version of this figure is available in the online journal.)

it should give a reasonable idea of the size of the effect. As we find below, the smallness of the claimed values for  $\frac{\Delta\alpha}{\alpha}$  imply that the uncertainties in  $q$ -values are not very important.

Table 2 shows the minimum values of  $\sigma_v$  for the portion of the combined 2004 spectra containing each of the transitions that have a calculated  $q$ -value. These results were calculated using co-added spectra from the standard XIDL HIRES pipeline that

did not include the iodine cell wavelength recalibration; this simplifies the calculation but has little effect on these minimum error results.

The values range from  $25 \text{ m s}^{-1}$  for the strong Fe II  $\lambda 1608$  line to  $153 \text{ m s}^{-1}$  for the weak lines such as Fe II  $\lambda 1611$ . It is interesting to note that the maximum velocity precisions obtainable with our data seem to be sufficient to measure the

**Table 2**  
Line Information

| Transition               | Echelle Order | $q$ value ( $\text{cm}^{-1}$ ) <sup>a</sup> | min $\sigma_v$ ( $\text{m s}^{-1}$ ) (2004 Data) | Iodine Cell Coverage? |
|--------------------------|---------------|---|--|-----------------------|
| Fe II $\lambda$ 1608.45  | 67            | $-1030 \pm 300^*$                           | 25.0   | Yes                   |
| Fe II $\lambda$ 1611.20  | 67            | $1560 \pm 500^*$                            | 153  | Yes                   |
| Al II $\lambda$ 1670.79  | 65            | $270 \pm ?\ddagger$                         | 34.0   | Yes                   |
| Ni II $\lambda$ 1709.60  | 63            | $-20 \pm 250^{**}$                          | 83.1   | Yes                   |
| Ni II $\lambda$ 1741.55  | 62            | $-1400 \pm 250^{**}$                        | 48.7   | Yes                   |
| Ni II $\lambda$ 1751.92  | 62            | $-700 \pm 250^{**}$                         | 70.8   | Yes                   |
| Si II $\lambda$ 1808.01  | 60            | $520 \pm 30^{**}$                           | 36.4   | Yes                   |
| Al III $\lambda$ 1854.72 | 58            | $458 \pm 2^{***}$                           | 76.0   | Yes                   |
| Al III $\lambda$ 1862.79 | 58            | $224 \pm 1^{***}$                           | 125  | Yes                   |
| Si II $\lambda$ 1526.71  | 71            | $50 \pm 30^{**}$                            | 28.8   | No                    |
| Zn II $\lambda$ 2026.14  | 53            | $2488 \pm 25^\dagger$                       | 129  | No                    |
| Zn II $\lambda$ 2062.66  | 52            | $1585 \pm 25^\dagger$                       | 229  | No                    |
| Cr II $\lambda$ 2056.26  | 52            | $-1030 \pm 150^{**}$                        | 89.9   | No                    |
| Cr II $\lambda$ 2062.24  | 52            | $-1168 \pm 150^{**}$                        | 102  | No                    |
| Cr II $\lambda$ 2066.16  | 52            | $-1360 \pm 150^{**}$                        | 143  | No                    |
| Fe II $\lambda$ 2344.21  | 46            | $1540 \pm 400^*$                            | 41.7   | No                    |

**Notes.**

<sup>a</sup>  $q$ -values marked \* are from Dzuba et al. (2002); marked \*\* from Porsev et al. (2007); marked † from Murphy et al. (2001a); marked ‡ from Savukov & Dzuba (2008); marked \*\*\* from Dzuba & Flambaum (2009).

shifts predicted by a changing value of  $\frac{\Delta\alpha}{\alpha}$  at the level claimed by Murphy et al. (2003). However, we also see that the weakness of the Fe II  $\lambda$ 1611 line means that the precision obtained from using only the Fe II  $\lambda$ 1608/ $\lambda$ 1611 pair may not be good enough for this purpose.

One can combine all these minimum  $\sigma_v$  values using Equation (3) to get an overall minimum velocity error, but since  $\frac{\Delta\alpha}{\alpha}$  is determined by differences in redshifts this is not appropriate. If one just wanted to determine how accurately the redshift of the entire system could be determined, then one could combine the minimum errors in Table 2 to find  $\sigma_v(\text{min})(\text{all}) = 13 \text{ m s}^{-1}$ . If we included only the lines for which we have iodine cell calibration the result is  $\sigma_v(\text{min})(\text{calib}) = 15 \text{ m s}^{-1}$ . The 2002 data alone would give  $38 \text{ m s}^{-1}$  precision, which if combined with the 2004 data would give an ultimate velocity precision of  $12 \text{ m s}^{-1}$ . Of course, as discussed below there are several important systematic errors that greatly increase these uncertainties.

Next we perform the least-squares fit to find minimum possible errors on  $\frac{\Delta\alpha}{\alpha}$  from this data and display the results in Table 3. These uncertainties, e.g.,  $\sigma(\frac{\Delta\alpha}{\alpha}) \geq 1.2 \times 10^{-6}$ , are reasonably competitive with errors quoted by Murphy et al. (2001a, 2003, 2004), with Chand et al. (2004), and with Levshakov et al. (2006). We again note that the latter two groups seem to have produced measurements of  $\frac{\Delta\alpha}{\alpha}$  with errors smaller than their minimum possible errors, something Murphy et al. (2008a) have criticized, and which Levshakov et al. subsequently corrected (Molaro et al. 2008).

We note that minimum possible error coming from analysis of the Fe II  $\lambda$ 1808/ $\lambda$ 1611 pair is  $\sigma(\frac{\Delta\alpha}{\alpha}) \geq 6.2 \times 10^{-6}$ , substantially less precise than could be found using several lines. As mentioned, this is mostly because the Fe II  $\lambda$ 1611 line is so weak (due to its rather low oscillator strength) and thus its redshift cannot be measured very precisely. Therefore, our original idea of using just these two lines is probably not that useful. In addition, examination of the lines shows that it is only the saturated regions of the Fe II  $\lambda$ 1608 line profile that are detectable in the Fe II  $\lambda$ 1611 line profile. Thus, a joint  $\chi^2$  fit cannot accurately recover their relative velocity offset. It seems it is better to com-

pare strong lines with other strong lines, and weak lines with other weak lines. We do this in the following section.

We can also test the importance of the uncertainties in  $q$  listed in Table 2, by doing a linear fit that allows errors in both the abscissa and ordinate. In this case, the resulting minimum error depends upon the fit value of  $\frac{\Delta\alpha}{\alpha}$ , that is, the slope of the line given in Equation (4). This is to be expected since if  $\frac{\Delta\alpha}{\alpha} = 0$ , it does not matter what the values of  $x$  are, while if there is a large slope then uncertainty in  $x$  will propagate to uncertainty in  $v$ , and therefore uncertainty in  $\frac{\Delta\alpha}{\alpha}$ . A simple way to estimate the increase in  $\frac{\Delta\alpha}{\alpha}$  uncertainty is to just do this propagation of errors, that is, change

$$\sigma_v^2 \rightarrow \sigma_v^2 + \left(\frac{\Delta\alpha}{\alpha}\right)^2 \sigma_x^2, \quad (5)$$

where  $\sigma_x = -2qc\lambda_0\sigma_q$ . The results of this error propagation are also shown in Table 3 for the Murphy et al. (2003) value  $\frac{\Delta\alpha}{\alpha} = -5.4 \times 10^{-6}$ . We note that because the slope  $\frac{\Delta\alpha}{\alpha}$  is small, the increase in uncertainty is also quite small, no larger than around 14% depending on the set of lines used. Thus, previous workers who ignored this effect are not making a large underestimation of their  $\frac{\Delta\alpha}{\alpha}$  uncertainties and limits. Because of the smallness of this effect, we will not consider the uncertainty in  $q$  in what follows.

It is important to realize that the minimum possible errors discussed above are never reached in a real observation for several reasons as follows.

1. As extensively discussed in Murphy et al. (2008b, Section 2.2.2), comparison between transitions with different degrees of saturation will give velocity uncertainties derived from Voigt profile fitting substantially greater than the Fisher matrix minimum. This is because velocity precision coming from the sharp edges of the saturated profiles cannot be directly compared with the central regions of unsaturated profiles. Especially in multicomponent systems, this will result in degeneracy between the component fit parameters, and make the redshift determination of any one component less accurate. This is evident when the

**Table 3**  
Minimum Possible Errors in  $\frac{\Delta\alpha}{\alpha}$

| Line Set                               | $\frac{\Delta\alpha}{\alpha}$ (min) (No Error in $q$ ) | $\frac{\Delta\alpha}{\alpha}$ (min) (Including Error in $q$ ) | $\frac{\Delta\alpha}{\alpha}$ (min) (No Error in $q$ ; w/o 12 exposures) |
|--|--|---|--|
| All 16 lines (2002 and 2004 data)      | $1.17 \times 10^{-6}$                                  | $1.32 \times 10^{-6}$   | ...  |
| All 16 lines                           | $1.21 \times 10^{-6}$                                  | $1.36 \times 10^{-6}$   | $1.50 \times 10^{-6}$  |
| Nine calibratable lines                | $2.00 \times 10^{-6}$                                  | $2.14 \times 10^{-6}$   | $2.52 \times 10^{-6}$  |
| Seven calibratable, unsaturated lines  | $2.69 \times 10^{-6}$                                  | $2.77 \times 10^{-6}$   | $3.28 \times 10^{-6}$  |
| Fe II $\lambda 1608/\lambda 1611$ pair | $6.18 \times 10^{-6}$                                  | $6.31 \times 10^{-6}$   | $6.20 \times 10^{-6}$  |

**Note.** Values are for 2004 data only and include exposures with and without the iodine cell in place, except where noted.

covariance matrix for one of our five component fits is examined. We see strong correlation between the redshifts of the various components and between these redshifts and various other parameters such as the  $b$ -values.

We can investigate this effect directly in our data by comparing the formal parameter fit errors with the minimum errors calculated above. For example, a five component fit of the saturated Fe II  $\lambda 1608$  line using the co-added data gives a minimum possible redshift error of  $33.4 \text{ m s}^{-1}$ , while the fitting program returns an error of  $184 \text{ m s}^{-1}$  on the strongest component.

For Si II  $\lambda 1808$ , an unsaturated line, the effect is smaller, but still pronounced:  $32.6 \text{ m s}^{-1}$  minimum error versus  $55 \text{ m s}^{-1}$  fit result. We note that the minimum errors found from using formulas (2) and (3) on the individual exposures are quite consistent with the minimum errors found from the co-added data. For three-component fit to Fe II  $\lambda 1608$ , we find  $32.6 \text{ m s}^{-1}$  for co-added data, versus  $27.4 \text{ m s}^{-1}$  from combining all seven non-iodine cell exposures. For Si II  $\lambda 1808$ , the comparison is  $50.4 \text{ m s}^{-1}$  from the co-added compared to  $49.9 \text{ m s}^{-1}$  for individual exposures. Note that errors returned from the fit software are actually also overly optimistic because.

- As discussed above there are other sources of error such as wavelength calibration.
- The errors on the flux are not really Gaussian which means that larger than Gaussian deviations occur.
- It is very difficult to determine the number of components needed to fit each transition, especially for saturated, or nearly saturated lines. The formal fit error returned on a component redshift does not include the possibility of another component, which may be apparent in some transitions and not in others. The  $\chi^2$  surface can have several local minima, and small measurement errors can switch one between needing another component and not needing another component. Since it is the difference between component redshifts that is used to determine  $\frac{\Delta\alpha}{\alpha}$ , this can be a source of systematic error. For example, we found examples where a region of a spectrum was formally slightly better fit by two nearby components than by a single component, but the redshift of the components in the two cases shifted by around  $1500 \text{ m s}^{-1}$ , a value large compared to what is expected from  $\frac{\Delta\alpha}{\alpha}$ .
- Murphy et al. (2008b) investigated this effect in detail (see their Figure 7) and found that while this effect does exist if the the number of fit components is less than the true number of components, this systematic error is greatly reduced if the number of fit components is equal to or greater than the true number of components.

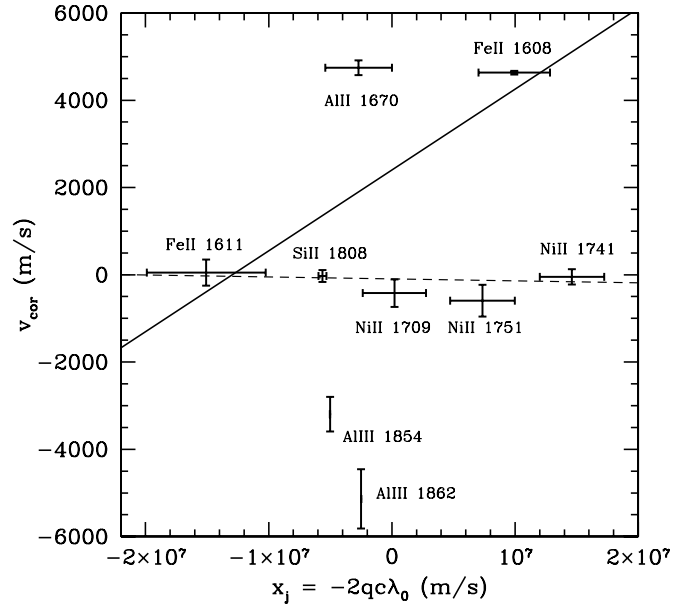


**Figure 10.** Linear fit simple method to find  $\frac{\Delta\alpha}{\alpha}$  for the strongest component of nine calibratable lines and non-iodine spectra. The solid line is the best fit for all nine lines, while the dashed line is the best fit for the five singly ionized unsaturated lines. The slope of the nine line fit is  $\frac{\Delta\alpha}{\alpha} = (186 \pm 6.3) \times 10^{-6}$ , and the slope of the five line fit is  $\frac{\Delta\alpha}{\alpha} = (-4.5 \pm 9.3) \times 10^{-6}$ .

### 3.3. Fitting for $\frac{\Delta\alpha}{\alpha}$ : Simple Method

We tried several methods of deriving a value of  $\frac{\Delta\alpha}{\alpha}$  from our Voigt profile fits. The simplest method is to fit each of our  $N$  lines independently, and then do a least squares linear fit of Equation (4). The value of  $v_j$  can be found from

$$v_j/c = (z_{\text{ave}} - z_j)/(1 + z_{\text{ave}}), \quad (6)$$

where  $z_{\text{ave}}$  is the redshift obtained by averaging over all the transitions detected in a given velocity component. The result of this simple direct method for component 1 (the component with the largest column density) of the nine lines for which we have both  $q$ -values, and an iodine spectrum is shown as the solid line in Figure 10. Here we plot  $x_j = -2q_j c \lambda_{0j}$  versus the wavelength corrected velocity  $v_{\text{cor}}$  for each line, as well as the best linear fit for the nine lines (solid line) and the best linear fit for the five unsaturated lines that are singly ionized (dashed line). For component 1 of the nine lines, the fit slope is  $\frac{\Delta\alpha}{\alpha}$  (component 1) =  $(186 \pm 6.3) \times 10^{-6}$ , with  $\chi^2/\text{d.o.f} = 264$ , formally a very strong detection, inconsistent with other measurements. For component 1 and the five lines, the fit slope is  $\frac{\Delta\alpha}{\alpha}$  (component 1) =  $(-4.5 \pm 9.3) \times 10^{-6}$ , with  $\chi^2/\text{d.o.f} = 1.09$ , formally a nice null result consistent with,

**Table 4**  
Fit Results for  $\frac{\Delta\alpha}{\alpha}$

| Method                    | Line Set  | $\frac{\Delta\alpha}{\alpha}/10^{-6}$ | $\chi^2/\text{d.o.f}$ | Probability ( $Q$ ) |
|---------------------------|---|---------------------------------------|-----------------------|---------------------|
| Simple (comp 1)           | The (5)   | $-4.5 \pm 9.3$                        | 1.09                  | 0.35                |
| Simple (comp 1)           | (5)+Fe II $\lambda 1608$                                      | $213 \pm 7.1$                         | 323                   | $10^{-278}$         |
| Simple (comp 1)           | (5)+Al III $\lambda 1854/\lambda 1862$                        | $6.7 \pm 9.2$                         | 22                    | $2 \times 10^{-22}$ |
| Simple (comp 1)           | (5)+Fe II $\lambda 1608$ + Al III $\lambda 1854/\lambda 1862$ | $237 \pm 6.8$                         | 248                   | $10^{-318}$         |
| Simple (comp 1)           | The (9)   | $186 \pm 6.3$                         | 264                   | 0                   |
| Simple (comp 2)           | The (5)   | $-7.1 \pm 12$                         | 0.66                  | 0.57                |
| Simple (comp 2)           | (5)+Fe II $\lambda 1608$                                      | $15 \pm 12$                           | 75                    | $10^{-63}$          |
| Simple (comp 2)           | The (9)   | $14 \pm 12$                           | 92                    | $10^{-136}$         |
| Simple (comp 3)           | (5)+Fe II $\lambda 1608$                                      | $25 \pm 51$                           | 3.8                   | 0.004               |
| Global joint fit          | Fe II $\lambda 1608$ and Fe II $\lambda 1611$ pair            | $-26 \pm 8.1$                         | 0.96                  | ...                 |
| Global joint fit          | The (5)   | $-3.3 \pm 4.3$                        | 0.80                  | ...                 |
| Global joint fit          | (5) + Fe II $\lambda 1608$                                    | $-18 \pm 3.8$                         | 0.92                  | ...                 |
| Global joint fit          | (5) + Al III $\lambda 1854/\lambda 1862$                      | $-6.3 \pm 4.3$                        | 0.83                  | ...                 |
| Global joint fit          | The (9)   | $-0.70 \pm 3.9$                       | 1.01                  | ...                 |
| VPFIT Global (w/o iodine) | (5) + Fe II $\lambda 1608$                                    | $-9.1 \pm 7.7$                        | 3.1                   | $10^{-39}$          |
| VPFIT Global (w/o iodine) | All 16  | $-17 \pm 10$                          | 6.0                   | 0                   |

**Notes.** The five (5) lines included in almost all the fits are Fe II  $\lambda 1611$ , Ni II  $\lambda 1709/\lambda 1741/\lambda 1751$ , and Si II  $\lambda 1808$ . The nine (9) lines are the (5) plus Fe II  $\lambda 1608$ , Al III  $\lambda 1854/\lambda 1862$  and Al II  $\lambda 1670$ . The VPFIT spectra were handled differently and did not include the iodine wavelength correction, so VPFIT results are not expected to be the same as our joint global fit results.

but much weaker than results in the literature, and a factor of 3 worse than the minimum possible error listed in Table 3.

However, we do not believe either of these results. If a changing fine structure were the explanation for the variation in values of  $v_{\text{cor}}$  in the nine line fit, then the points in Figure 10 would lie on a straight line within errors. We see from the figure and from the terrible  $\chi^2/\text{d.o.f}$  that this is not the case. When the goodness of fit to a model is very bad, it means that either the model is incorrect or that there are systematic errors not included in the data uncertainties. In such cases, the errors derived from the fit cannot be trusted, and a better way to estimate the uncertainty is to increase the errors on the data points until  $\chi^2/\text{d.o.f} \approx 1$ . Doing this for the nine line fit gives  $\frac{\Delta\alpha}{\alpha}(\text{component 1}) = (186 \pm 102) \times 10^{-6}$  ( $\chi^2/\text{d.o.f} = 1.01$ ), a null result with a more realistic error estimate, but far from the sensitivity we expected from our data.

Another way to see that the first result above is meaningless is to do the fit including the errors in  $q$ . This gives an entirely different answer which also is a terrible fit. However, when the errors are scaled as above, this fit then gives nearly the same result as above but with larger errors.

The problem with the nine line fit seems to be the saturated lines Fe II  $\lambda 1608$  and Al II  $\lambda 1670$ , as well as the aluminum lines Al III  $\lambda 1854$  and  $\lambda 1862$ . Since Al III is in a different ionization state than the other ions, it might exist at a different physical location, and so maybe should be left out of the fits. We want to discuss in more detail the saturated lines that are far from the others, but before doing that we note that this pattern repeats also in the  $x$  versus  $v_{\text{cor}}$  fits of the 2nd strongest component, the results of which are given in Table 4.

The fit redshifts of the first components of the Fe II  $\lambda 1608$  and Al II  $\lambda 1670$  lines differ from the dashed five line fit by about  $\Delta z \sim 5 \times 10^{-5}$ . Some insight into possible reasons for this can be gained by noting that if we force this component of Fe II  $\lambda 1608$  to be the same as the average of the unsaturated transitions, we also get a completely satisfactory fit to the Voigt profile:  $\chi^2/\text{d.o.f} = 1487.7/1495 = .995$  for the free fit, and  $\chi^2/\text{d.o.f} = 1503.4/1496 = 1.004$  ( $Q = 0.43$ ) for the 3 component fit with one redshift forced to the average value. The reported formal fit errors on these redshifts are

$\sigma_z = 4.4 \times 10^{-7}$ , substantially smaller than the difference between the free fit and the forced fit. Thus, we see another possible source of error in determining  $\frac{\Delta\alpha}{\alpha}$ . The formal fit errors seem to underestimate the true range of acceptable redshift values, and therefore overestimate the precision with which  $\frac{\Delta\alpha}{\alpha}$  can be determined by this method. We note that when we force the redshift of the first component of Fe II  $\lambda 1608$  to agree with the other lines, the second and third component also come into alignment. Thus there is a degeneracy where the redshift and  $b$ -value of one component can play off the redshift and  $b$ -values of other components. Another way this can be seen, is from the fact that the value derived for  $\frac{\Delta\alpha}{\alpha}$  depends greatly on the error reported for the Fe II  $\lambda 1608$  redshift. Figure 10 shows that the linear fit for  $\frac{\Delta\alpha}{\alpha}$  is driven by the tiny error on the Fe II  $\lambda 1608$  redshift. Increasing that error by a factor of 10 (to roughly equal the errors on the other redshifts) changes the value to  $\frac{\Delta\alpha}{\alpha} = (-9.3 \pm 9.0) \times 10^{-6}$ .

Examination of the Al II  $\lambda 1670$  line shows a similar problem; again the line is saturated and in this case there are certainly more than three detectable components. We are only allowing three total components so that we can compare component to component across other transitions where only three components are detectable, but the fitting program can find different nearly equivalent ways to fit the line to three components since saturation means less shape information is available.

While the effect is largest for the saturated lines, we find the same effect for the Al III  $\lambda 1864$  and Al II  $\lambda 1862$ , unsaturated lines, where there are only three detectable components. Here again while the best fit redshift is far from the others, we can get a completely acceptable fit to the Voigt profile ( $\chi^2/\text{d.o.f} < 1$ ) even while forcing the first component to the average. Again, when one component is forced to agree, the other components then also agree.

Thus, we note a systematic error that can give trouble in this type of fitting. When a system has two (or more) components nearby in redshift space, there can be a near degeneracy where the two redshifts can play off each other, moving significantly at the level of precision we are after, but yet still giving very good Voigt profile fits.

**Table 5**  
Component Fit Values for a 3 Component Joint Global Fit of 9 Lines

| Component | Redshift $z$                                   | Velocity Width $b$ (km s <sup>-1</sup> ) | Log Column Density $\log(N)$ |
|-----------|--|--|------------------------------|
| Comp 1    | 2.3090291 $\pm$ 9.58 $\times$ 10 <sup>-7</sup> | 6.41 $\pm$ 0.05                          | 14.76 $\pm$ 0.029            |
| Comp 2    | 2.3091517 $\pm$ 1.68 $\times$ 10 <sup>-6</sup> | 7.75 $\pm$ 0.12                          | 14.563 $\pm$ 0.035           |
| Comp 3    | 2.3094793 $\pm$ 9.49 $\times$ 10 <sup>-7</sup> | 16.44 $\pm$ 0.11                         | 14.039 $\pm$ 0.021           |

**Notes.** The nine lines included in the fit are the ones listed in the introduction. Each component of each element has an additional fit parameter (not listed) which is a column density offset to allow for different elemental abundances. This fit resulted in a fit value of  $\frac{\Delta\alpha}{\alpha} = (-0.070 \pm 3.9) \times 10^{-6}$  and  $\chi^2/\text{d.o.f} = 14138/13891 = 1.01$ .

Note that a linear fit to the five line set that includes the  $q$  errors gives nearly the same answer as shown by the dashed line in Figure 10. This is to be expected since the slope of the line,  $\frac{\Delta\alpha}{\alpha}$ , is small.

We can repeat the above analysis for the second and third strongest components. The results are given in Table 4 for various sets of lines. In these cases, we mostly find null results such as  $\frac{\Delta\alpha}{\alpha}$  (component 2) =  $(14 \pm 12) \times 10^{-6}$  with  $\chi^2/\text{d.o.f} = 92$  for all nine lines. This is because the lower column densities mean larger formal fit errors.

There are additional components detectable in some of the lines, but they are much weaker and do not contribute much. To get a final answer using this method, one could average the above results, which actually gives a result with larger formal error than from the first component alone, again showing that systematic errors are dominating this procedure.

### 3.4. Fitting for $\frac{\Delta\alpha}{\alpha}$ : Many Parameter Joint Fit

The above method, while useful for showing errors arising from fitting degeneracies, is not really correct because for it to work one must match up the various components fit in different lines in order to properly compare their redshifts. As noted, these fitting degeneracies allow the redshifts of two nearby components to be traded against each other and against the  $b$ -values, resulting in correlations that cause the uncertainty in the component redshifts to be larger than the formal fit errors.

More properly, one should do a large joint fit for all system components simultaneously, that is tie together the different velocity components. This is standard practice and is used by Murphy et al., Chand et al., Levshakov et al., etc. Thus, for example, the fit to the nine lines above by the previous method used a total of 81 parameters: redshift, column density and  $b$ -value for each of three components of each of nine lines. A global joint fit might have nine parameters for the redshift, column density, and  $b$ -value of each of three components, plus some column density offsets to allow for different elemental abundances (one-parameter per component per additional element or 12 including Fe II, Ni II, Si II, and Al II and Al III). An additional  $b$ -value offset is probably necessary for each component of the Al III lines since these are in a different ionization state (three more parameters). Then adding  $\frac{\Delta\alpha}{\alpha}$  as a final parameter, there would be a total of 25 parameters.

The results of such a global joint fit method are shown in Table 4 for various sets of lines. Table 4 shows that results we find for  $\frac{\Delta\alpha}{\alpha}$  vary over a wide range of values from significant detection  $\frac{\Delta\alpha}{\alpha} = (-26 \pm 8) \times 10^{-6}$  for the Fe II  $\lambda 1608$ /Fe II  $\lambda 1611$  pair to a null result  $\frac{\Delta\alpha}{\alpha} = (-0.07 \pm 3.9) \times 10^{-6}$  for the nine-line fit. Looking over all the results in Table 4, we see that both the method used and the lines selected can make a significant difference in the final result. If our errors were under

control, this should not be the case. Note that in most cases, the errors for the global fit method hover around  $4 \times 10^{-6}$ ; roughly half the errors of around  $8 \times 10^{-6}$  found in the simple method described in the previous section. In Table 5, we display the Voigt profile components that resulted from one of our joint global fits.

### 3.5. Fitting for $\frac{\Delta\alpha}{\alpha}$ : VPFIT Global Joint Fit

One might worry that the puzzling results we find come from errors in our fitting program, so as a final check, we redid our calculation of  $\frac{\Delta\alpha}{\alpha}$  using the new version of VPFIT (Carswell et al. 2008) which includes the possibility of doing a global joint fit for  $\frac{\Delta\alpha}{\alpha}$ . These results are also shown in Table 4. For the six line set (Fe II  $\lambda 1611/\lambda 1608$ , Ni II  $\lambda 1709/\lambda 1741/\lambda 1751$ , Si II  $\lambda 1808$ ) we studied above we find  $\frac{\Delta\alpha}{\alpha} = (-9.1 \pm 7.7) \times 10^{-6}$  ( $\chi^2/\text{d.o.f} = 3.1$ ,  $Q = 5 \times 10^{-69}$ ), while for the set of all 16 lines we find  $\frac{\Delta\alpha}{\alpha} = (-17 \pm 10) \times 10^{-6}$  ( $\chi^2/\text{d.o.f} = 6.0$ ,  $Q = 0$ ). Both these results are within the range found by our different fitting methods.

## 4. DISCUSSION

We tried and failed to give a definitive answer to the question of whether the fine structure constant was different at early times in high redshift Ly $\alpha$  systems. In order to investigate this problem in detail, we used data taken through the Keck iodine cell and wrote our fitting software from scratch. Using the iodine cell for wavelength calibration, we found a serious source of systematic error that did not allow calibration of the Keck HIRES spectrograph to the precision needed. We also found degeneracies in the fitting procedures that added to the calibration systematic errors.

Due to all the systematic errors, we were able to derive various results, running from very significant detections, to strong null limits. Does this imply that a meaningful measurement of or limit on  $\frac{\Delta\alpha}{\alpha}$  is impossible using Keck HIRES? It is not clear. Perhaps more careful attention to Voigt profile fitting, as advocated by M. Murphy (2008, private communication) will solve the fit degeneracy problem. Perhaps a careful selection of absorbers would also help, or trying to focus on systems with a single component. Perhaps the wavelength calibration errors we discovered can be corrected, or perhaps they will average away if a large sample of absorbers is considered. In this paper, we raise these questions, but do not answer them.

We also used a Fisher matrix technique to investigate the minimum possible errors in  $\frac{\Delta\alpha}{\alpha}$  that our spectra's S/N would allow. We found our fit results did not exceed these limits. For example, for the set of nine lines used in most of our analyses, the minimum possible error on  $\frac{\Delta\alpha}{\alpha}$ , as given in Table 3, is  $2.52 \times 10^{-6}$ , a result consistent with our fit results. Since the calculation of minimum possible errors is not difficult,

we suggest that workers always calculate them and never report results with uncertainties smaller than the data theoretically can allow.

While we have not yet looked carefully at data or analysis done by other workers in the field, we worry that some of the systematic errors and overestimation of precision we found here may also be present in other analyses. Thus, one possible explanation for the discrepant findings on  $\frac{\Delta\alpha}{\alpha}$  discussed in the introduction is that several workers in the field are overestimating the precision of their measurements and the discrepancies reported in the literature are due to random fluctuations occurring within the larger, under-reported, systematic errors.

At this point, it is not clear how to make further progress in this subject using Keck HIRES, but other techniques such as frequency combs (Steinmetz et al. 2008) may become available and be of use in resolving the question. In addition, proposed new instruments (e.g., CODEX for E-ELT or ESPRESSO for the VLT) are being designed for Doppler measurement stability and will hopefully be free of these problems.

We thank David Kirkman, Bob Carswell, Marc Rafelski, Joel Heinrich, John Johnson, and Michael J. Simmonds for helpful discussions. We especially thank Michael Murphy for many insightful comments, suggestions and questions, including several that led to corrections of errors in early versions of this paper. Finally, we thank Nao Suzuki for discussion of an early version of this paper where we discovered that he had already understood and published several of the points made here.

K.G. and J.B.W. were supported in part by the DoE under grant DE-FG03-97ER40546. J.X.P. is partially supported by an NSF CAREER grant (AST-0548180), and J.X.P. and A.M.W. are supported in part by NSF grant (AST-07-09235). The W. M. Keck Observatory is operated as a scientific partnership among the California Institute of Technology, the University of California and the National Aeronautics and Space Administration. The Observatory was made possible by the generous financial

support of the W. M. Keck Foundation. The authors recognize and acknowledge the very significant cultural role and reverence that the summit of Mauna Kea has always had within the indigenous Hawaiian community. We are most fortunate to have the opportunity to conduct observations from this mountain.

## REFERENCES

- Barlow, T. 2002, MAKEE Keck Observatory HIRES Data Reduction Software (Pasadena, CA: Caltech), <http://spider.ipac.caltech.edu/staff/tab/makee/index.html>
- Beaver, E. A., et al. 1972, *ApJ*, **178**, 95
- Bouchy, F., Pepe, F., & Queloz, D. 2001, *A&A*, **374**, 733
- Butler, R. P., et al. 1996, *PASP*, **108**, 500
- Carswell, R. F., Webb, J. K., Cooke, A. J., & Irwin, M. J. 2008, VPFIT version 9.5, <http://www.ast.cam.ac.uk/~rfc/vpfit.html>
- Chand, H., et al. 2004, *A&A*, **417**, 853
- Dzuba, V. A., & Flambaum, V. V. 2009, *Can. J. Phys.*, **87**, 15
- Dzuba, V. A., Flambaum, V. V., Kozlov, M. G., & Marchenko, M. 2002, *Phys. Rev. A*, **66**, 022501
- Garcia-Berro, E., Isern, J., & Kubyshev, Y. A. 2007, *A&AR*, **14**, 113
- Kirkman, D., et al. 2003, *ApJS*, **149**, 1
- Levshakov, S. A., et al. 2007, *A&A*, **466**, 1077
- Levshakov, S. A., et al. 2006, *A&A*, **449**, 879
- Molaro, P., Reimers, D., Agafonova, I. I., & Levshakov, S. A. 2008, *Eur. Phys. J. Spec. Top.*, **163**, 173
- Murphy, M. T., et al. 2001a, *MNRAS*, **327**, 1208
- Murphy, M. T., et al. 2004, *Astrophysics, Clocks, and Fundamental Constants*, ed. S. G. Karshenboim & E. Peik (Berlin: Springer), 131
- Murphy, M. T., Webb, J. K., Flambaum, V. V., Churchill, C. W., & Prochaska, J. X. 2001b, *MNRAS*, **327**, 1236
- Murphy, M. T., Webb, J. K., & Flambaum, V. V. 2003, *MNRAS*, **345**, 609
- Murphy, M. T., Webb, J. K., & Flambaum, V. V. 2008a, in *Proc. Precision Spectroscopy in Astrophys.*, ed. N. C. Santos et al. (Garching: ESO), 95
- Murphy, M. T., Webb, J. K., & Flambaum, V. V. 2008b, *MNRAS*, **384**, 1053
- Osterbrock, D. E., et al. 2000, *PASP*, **112**, 733
- Porsev, S. G., et al. 2007a, *Phys. Rev. A*, **76**, 052507
- Porsev, S. G., et al. 2007b, *MNRAS*, **384**, 1053
- Savukov, I. M., & Dzuba, V. A. 2008, *Phys. Rev. A*, **77**, 042501
- Srianand, R., Chand, H., Petitjean, P., & Aracil, B. 2004, *Phys. Rev. Lett.*, **92**, 121302
- Steinmetz, T., et al. 2008, *Science*, **321**, 1335
- Suzuki, N., et al. 2003, *PASP*, **115**, 1050
- Wells, R. J. 1999, *J. Quant. Spectrosc. Radiat. Transfer*, **62**, 29